Physica D 240 (2011) 346–356

Contents lists available at ScienceDirect

Physica D

journal homepage: www.elsevier.com/locate/physd

Weakly nonlinear non-Boussinesq internal gravity wavepackets

H.V. Dosser, B.R. Sutherland *

Department of Physics, University of Alberta, Edmonton, AB, T6G 2G7, Canada

ARTICLE INFO

Article history:
Received 15 July 2009
Received in revised form
9 June 2010
Accepted 20 September 2010
Available online 25 September 2010
Communicated by J. Bronski

Keywords:
Internal gravity waves
Schrödinger equation
Modulational stability

ABSTRACT

Internal gravity wavepackets induce a horizontal mean flow that interacts nonlinearly with the waves if they are of moderately large amplitude. In this work, a new theoretical derivation for the wave-induced mean flow of internal gravity waves is presented. Using this we examine the weakly nonlinear evolution of internal wavepackets in two dimensions. By restricting the two-dimensional waves to be horizontally periodic and vertically localized, we derive the nonlinear Schrödinger equation describing the vertical and temporal evolution of the amplitude envelope of non-Boussinesq waves. The results are compared with fully nonlinear numerical simulations restricted to two dimensions. The initially small-amplitude wavepacket grows to become weakly nonlinear as it propagates upward due to non-Boussinesq effects. In comparison with the results of fully nonlinear numerical simulations, the nonlinear Schrödinger equation is found to capture the dominant initial behaviour of the waves, indicating that the interaction of the waves with the induced horizontal mean flow is the dominant mechanism for weakly nonlinear evolution. In particular, due to modulational stability, hydrostatic waves propagate well above the level at which linear theory predicts they should overturn, whereas strongly non-hydrostatic waves, which are modulationally unstable, break below the overturning level predicted by linear theory.

1. Introduction

Internal gravity waves exist in stably stratified fluids, in which the effective density decreases continuously with height. Examples of such fluids include a liquid such as the ocean, where salinity and temperature vary, or a gas such as the atmosphere, where the effective density is determined by the temperature and thermodynamics of the fluid. For a fluid in which the density does not change significantly relative to the total depth, it is typical to apply the Boussinesq approximation. In this approximation, the background density is taken to be constant in the governing equations for internal waves, with the exception of the buoyancy term in the momentum conservation equation [1]. Together with the requirement of incompressibility, this has the effect of filtering sound waves from the fluid. Typically, the Boussinesq approximation is used for the ocean, since the change in background density over its total depth is small. For the atmosphere, waves propagating upwards over a significant height experience a large background density decrease, so their evolution is governed by non-Boussinesq processes. In particular, due to momentum conservation, small amplitude waves launched near the ground, which initially obey linear theory, grow as they propagate upwards [2] and eventually reach such large amplitudes that linear theory no longer adequately models their evolution. These moderately large amplitude waves require the use of a weakly nonlinear theory to accurately capture their evolution.

Despite the importance of nonlinear effects upon the evolution and ultimately the breaking of internal gravity waves, developing a weakly nonlinear theory for moderately large amplitude waves has been challenging because plane wave solutions of the linear equations are also exact solutions of the fully nonlinear equations of fluid motion. Recently however, a new approach that examines wavepackets was successfully employed to predict the evolution of weakly nonlinear Boussinesq waves [3]. One purpose of this paper is to extend these results to non-Boussinesq waves and, together with fully nonlinear numerical simulations, test the range of validity of linear theory.

Previous studies which considered the amplitude growth of vertically propagating internal gravity waves often focused on wave interactions with an existing background mean flow. It was found that transient internal waves could modify this mean flow, changing the breaking height of any subsequent waves, as demonstrated by Dunkerton through quasi-linear numerical simulations [4]. Fully nonlinear simulations by Grimshaw displayed differences in the evolution of small and large amplitude Boussinesq internal waves due to interactions with a wind shear and Doppler-shifting of the waves by the mean flow [5]. In the absence of any initial background shear, numerical investigations by Jones & Houghton showed that, although linear theory could correctly predict the breaking height of the initial wave, energy transfer to the mean flow during wave overturning modified the breaking heights of any further waves [6].

* Corresponding author. Tel.: +1 780 492 0573; fax: +1 780 492 0714.
E-mail address: bruce.sutherland@ualberta.ca (B.R. Sutherland).

0167-2789/$ – see front matter © 2010 Elsevier B.V. All rights reserved.
doi:10.1016/j.physd.2010.09.008

Even in the absence of any background shear or mean flow created by wave breaking events, there will still be interactions between the waves and the transient horizontal mean flow created by the waves themselves. Within a wavepacket that is horizontally periodic and vertically localized, the wave components interact with each other in such a way that a mean flow is induced during propagation. This mean flow is the horizontally averaged horizontal flow, whose vertical profile translates upwards with the wavepacket as it propagates. This 'wave-induced mean flow' is present as soon as the waves are generated, and is analogous to the Stokes' drift for surface waves. The Stokes' drift is a second order amplitude effect, which causes the mean velocity of a fluid parcel to be non-zero [1].

Using Hamiltonian fluid mechanics, a form for the wave-induced mean flow of internal waves in a Boussinesq fluid was determined by identifying the wave-induced mean flow as the pseudomomentum per unit mass [7]. The pseudomomentum is a conserved quantity, provided that the fluid through which the waves propagate is invariant with respect to translations [8]. In this sense, it replaces the momentum of the waves, which is not conserved for waves propagating through a medium. This connection with the pseudomomentum resulted in an explicit formula for the wave-induced mean flow of a two-dimensional wavepacket, given at leading order by

$$U(z,t) \equiv -\langle \xi \zeta \rangle, \tag{1}$$

in which ξ is the vertical displacement of the fluid caused by the waves, ζ is the vorticity, defined as the spanwise component of the curl of the wave velocity, and the average is taken over one horizontal wavelength. This form for the wave-induced mean flow is accurate for small amplitude waves in a Boussinesq fluid, and has previously been shown to be a reasonably good approximation even for waves of moderately large amplitude [9].

Although the Stokes' drift does not significantly impact the evolution of surface waves, interactions between internal waves and their wave-induced mean flow have been shown to dominate the evolution of Boussinesq internal gravity wavepackets for amplitudes below breaking [10,11]. The nature of the interaction has been referred to as 'self-acceleration' [12]. The wave-induced mean flow acts to Doppler-shift the frequency of the waves significantly from linear theory values, if the waves are of moderately large amplitude. This can increase the transmission of a sufficiently large-amplitude Boussinesq wavepacket across a reflecting level [13] and can modify the level at which the waves overturn and break [14]. Wave breaking due to self-acceleration has been seen to occur if the wave-induced mean flow is greater than the horizontal component of the group velocity of the waves. All of these results focused upon Boussinesq waves with large initial amplitude. In this work, we will be focusing on the evolution of a wavepacket with small initial amplitude, which grows to large amplitude during its propagation due to non-Boussinesq effects.

The physics that dictate how weak nonlinearity affects non-Boussinesq internal gravity waves as they grow from small to large amplitude is given by the nonlinear Schrödinger equation. This partial differential equation describes the spatial and temporal evolution of the amplitude envelope of moderately large amplitude waves. A linear Schrödinger equation for a horizontally periodic and vertically localized wavepacket that includes the effect of translation at the group velocity has the form:

$$\partial_t A + c_{gz}\partial_z A = \imath \frac{1}{2}\omega_{mm}\partial_{zz}A, \tag{2}$$

in which $A(z,t)$ specifies the shape of the wavepacket envelope, $c_{gz} \equiv \omega_m$ and ω_{mm} are constant coefficients determined from taking m derivatives of the dispersion relation $\omega = \omega(m,k)$, in which m and k are the vertical and horizontal wavenumbers respectively. The quantity c_{gz} is the vertical (component of the) group velocity which denotes the speed at which a small amplitude quasi-monochromatic wavepacket translates vertically. Because the wavepacket is horizontally periodic its horizontal translation is ignored. Thus the linear equation captures only the vertical translation of the wavepacket at the group velocity and the effects of leading order linear dispersion upon small amplitude waves. Nonlinearity is introduced by including the effects of self-acceleration and higher order nonlinear dispersion. The form for the wave-induced mean flow given by Eq. (1) was recently used in the derivation of a weakly nonlinear Schrödinger equation describing the evolution of an internal gravity wavepacket in a Boussinesq fluid [3]. However, Eq. (1) is not valid for internal gravity waves in a non-Boussinesq fluid. In order to derive the Schrödinger equation for a non-Boussinesq fluid, it is necessary to determine the appropriate form for the wave-induced mean flow.

The wave-induced mean flow for two-dimensional Boussinesq wavepackets has been derived previously using energy conservation relations. Bretherton [15] used the polarization relations to relate the vertical flux of horizontal mean momentum per unit mass to the wave energy density E via:

$$\langle uw \rangle = \left(\frac{\langle E \rangle}{\omega - k\bar{U}} \right) k c_{gz} \tag{3}$$

in which u, w are the horizontal and vertical components of the fluctuation velocity, c_{gz} is the vertical group velocity of the wave, k is the horizontal wavenumber, and $\bar{U}(z)$ is the prescribed horizontal background velocity. The term in parentheses in Eq. (3) is $\mathcal{A}$, the wave-action density [16].

Separately, Acheson [17] derived an equation relating the wave energy density to the wave-induced mean flow:

$$U = \frac{\langle E \rangle}{\omega - k\bar{U}} k = \mathcal{A} k. \tag{4}$$

The derivation of this equation takes advantage of the conservation of wave action, and a heuristic comparison of terms resulting from the polarization relations. In combination, Eqs. (3) and (4) result in a succinct relation for the wave-induced mean flow $U(z,t)$:

$$\langle uw \rangle = c_{gz} U(z,t). \tag{5}$$

In part, this paper will develop a more intuitive method to derive a formula for the wave-induced mean flow based upon momentum rather than energy or wave action conservation laws. Such an approach to the derivation of the wave-induced mean flow equations is consistent with the general formulation of Andrews & McIntyre [18] who derived the Lagrangian-mean equations for energy and momentum conservation laws, though not specifically for internal waves. From our equation for the wave-induced mean flow, we derive the corresponding nonlinear Schrödinger equation describing the evolution of non-Boussinesq internal gravity wavepackets. This equation allows us to assess the modulational stability of the waves [19,20].

Modulational stability and instability are weakly nonlinear effects occurring for dispersive wavepackets. The amplitude envelope of modulationally unstable waves initially narrows and its peak value grows whereas modulationally stable waves spread faster than the rate resulting from linear dispersion alone [19]. The manifestation of weakly nonlinear modulational effects upon non-Boussinesq internal waves has non-trivial and potentially atmospherically relevant consequences. Linear theory predicts non-Boussinesq waves grow in amplitude with height, eventually breaking when they reach overturning amplitudes. We anticipate that the peak amplitude of upward propagating modulationally unstable wavepackets will grow faster than predicted by linear theory and so cause the waves to break at

lower levels than the overturning level predicted by linear theory. Likewise modulationally stable waves are expected to propagate without breaking to higher levels than the overturning level predicted by linear theory. However, even in weakly nonlinear theory, this anticipated result is not obvious. It is possible for a modulationally unstable wavepacket to avoid breaking through the Fermi–Pasta–Ulam recurrence phenomenon [21], in which a periodic transfer of energy among the wavenumber components is followed by a return to the initial state. This phenomenon has been observed numerically using a nonlinear Schrödinger equation for a deep water wave train experiencing the Benjamin–Feir instability [22,23]. Through the inclusion of higher order terms in our weakly nonlinear Schrödinger equation, we will show that higher order linear and nonlinear dispersion breaks the symmetry associated with Fermi–Pasta–Ulam recurrence. The inclusion of higher order terms has previously been shown to improve the modelling of the nonlinear evolution of a deep water wave train [24], particularly in capturing the Doppler-shifting of the wave by the induced mean flow.

Though not captured by the nonlinear Schrödinger equation, internal waves may also transfer energy to waves of shorter wavelength and higher wavenumber through parametric subharmonic instability [25,26]. This instability results from an interaction between three waves, in which energy is transferred from the primary wave to two other secondary waves of fractional frequency [16]. It can lead to wave steepening and overturning as energy cascades to smaller scales [27]. However, in our weakly and fully nonlinear equations, the secondary waves are not present at the outset and must grow out of noise. Thus it takes substantial time for the secondary waves to grow to such amplitude that they substantially affect the primary wave through parametric subharmonic instability. On the other hand, the wave-induced mean flow is manifest in tandem with an internal wavepacket at the outset and so can immediate influence the wavepacket evolution through weakly nonlinear modulations [10]. It is therefore anticipated that modulational instability will emerge as the primary mechanism determining the evolution of a wavepacket moving upwards through a non-Boussinesq fluid.

In Section 2, a simple form for the wave-induced mean flow is derived through a wavepacket approach. Using a similar procedure, the corresponding nonlinear Schrödinger equation for internal gravity wavepackets in a non-Boussinesq liquid is derived. The numerical methods used to integrate this equation are described in Section 3 as are the details of the fully nonlinear numerical simulations. Weakly and fully nonlinear results are compared in Section 4. The breaking levels predicted by linear theory are then compared with the results from the fully nonlinear numerical simulations in Section 5. Conclusions regarding the influence of the wave-induced mean flow on internal gravity wavepacket growth, development, and breaking height are drawn in Section 6.

2. Theory

The fully nonlinear non-Boussinesq equations for inviscid, two-dimensional internal gravity waves in a stationary non-rotating liquid are given by

$$\bar{\rho}\frac{D\vec{u_T}}{Dt} = -\nabla p - g\rho\hat{z} \tag{6}$$

$$\nabla\cdot\vec{u_T} = 0 \tag{7}$$

$$\frac{D\rho_T}{Dt} = 0. \tag{8}$$

Here $\vec{u_T} = (u_T, w_T)$ denotes the total horizontal and vertical velocities, respectively, and the total density $\rho_T(x,z,t)$ is the sum of the background density, $\bar{\rho}(z)$ and the fluctuation density associated with the waves, $\rho(x,z,t)$. Eq. (6) represents momentum conservation for an inviscid fluid, (7) is the mass conservation equation for an incompressible liquid, and (8) is the equation for conservation of internal energy in which the effects of diffusion are neglected. Background hydrostatic balance, $\partial\bar{p}/\partial z = -\bar{\rho}g$, in which the gravitational term in the momentum conservation equation (6) is balanced by the background pressure gradient term [28], has been assumed so that only the fluctuation pressure, p, appears. The material derivative is $D/Dt = \partial_t + u_T\partial_x + w_T\partial_z$. Eq. (7) has the effect of filtering sound waves in a liquid, and results from the need for self-consistency between the internal energy equation and the incompressibility condition for a liquid, both of which have the form:

$$\frac{D\rho_T}{Dt} = 0. \tag{9}$$

It follows from the continuity equation in its general form

$$\frac{D\rho_T}{Dt} = -\rho_T\nabla\cdot\vec{u_T} \tag{10}$$

that (7) is satisfied. The equations for a non-Boussinesq liquid differ from the Boussinesq equations only in the appearance of $\bar{\rho}$, rather than a characteristic density ρ_0, multiplying the acceleration terms in (6).

In order to determine the dispersion relation for internal gravity waves in a non-Boussinesq liquid, we first linearize the equations of motion as follows:

$$\bar{\rho}\frac{\partial\vec{u_T}}{\partial t} = -\nabla p - g\rho\hat{z} \tag{11}$$

$$\nabla\cdot\vec{u_T} = 0 \tag{12}$$

$$\frac{\partial\rho}{\partial t} = -w\frac{\mathrm{d}\bar{\rho}}{\mathrm{d}z}. \tag{13}$$

The components of the total horizontal and vertical velocity fields are given in terms of a scalar function, the total streamfunction ψ_T, by $u_T = -\partial_z\psi_T$ and $w_T = \partial_x\psi_T$, respectively. The total vorticity field corresponding to the streamfunction is $\zeta_T \equiv \partial_z u_T - \partial_x w_T = -\nabla^2\psi_T$. Thus, the linearized momentum conservation equations can be recast as one equation for the total streamfunction and fluctuation density

$$\frac{\partial}{\partial t}\nabla^2\psi_T = -\frac{g}{\bar{\rho}}\frac{\partial\rho}{\partial x} - \frac{1}{\bar{\rho}}\frac{\mathrm{d}\bar{\rho}}{\mathrm{d}z}\frac{\partial^2\psi_T}{\partial t\partial z}. \tag{14}$$

Using (13) to eliminate ρ leads to the equation

$$\frac{\partial^2}{\partial t^2}\nabla^2\psi = -\frac{g}{H}\frac{\partial^2\psi}{\partial x^2} + \frac{1}{H}\frac{\partial^3\psi}{\partial t^2\partial z}, \tag{15}$$

where H is the density scale height in the fluid, defined by

$$H \equiv -\left(\frac{1}{\bar{\rho}}\frac{\mathrm{d}\bar{\rho}}{\mathrm{d}z}\right)^{-1}. \tag{16}$$

In (15) we require that there be no background motion independent of the waves, so that the fluctuation streamfunction is equal to the total streamfunction, $\psi = \psi_T$.

We assume the fluid is uniformly stratified so that $\bar{\rho} = \rho_0\exp(-z/H)$. The squared buoyancy frequency, given by $N^2 \equiv -(g/\bar{\rho})\mathrm{d}\bar{\rho}/\mathrm{d}z = g/H$, is therefore constant. Following a standard procedure (for example see Gill [16]) the frequency of small amplitude non-Boussinesq internal waves, given by the dispersion relation, is found to be:

$$\omega = N\frac{k}{\left(k^2 + m^2 + \frac{1}{4H^2}\right)^{1/2}}, \tag{17}$$

Table 1
Polarization relations for small amplitude internal gravity waves in a non-Boussinesq liquid.

Defining formula	Relationship to ψ
ψ	A_ψ
$u = -\partial_z\psi$	$A_u = -\left(\imath m + \frac{1}{2H}\right)A_\psi$
$w = \partial_x\psi$	$A_w = -\imath k A_\psi$
$\zeta = -\nabla^2\psi$	$A_\zeta = \left(k^2 + m^2 - \frac{1}{4H^2} - \imath\frac{m}{H}\right)A_\psi$
$w = \frac{\partial\xi}{\partial t}$	$A_\xi = -\frac{k}{\omega}A_\psi$
$\xi \approx H\frac{\rho}{\bar\rho}$	$A_\rho \approx -\bar\rho\frac{k}{H\omega}A_\psi$

in which k and m are the horizontal and vertical wavenumbers respectively. This form for the dispersion relation is identical to that for small amplitude internal waves in an anelastic gas. The streamfunction of a plane wave has the form

$$\psi = A_\psi \exp\left[\imath(kx + mz - \omega t) + z/2H\right] + c.c. \tag{18}$$

in which A_ψ is one-quarter of the peak-to-peak streamfunction amplitude of the wave and $c.c.$ denotes the complex conjugate. The polarization relations of other fields are listed in Table 1.

If we consider the advective terms in the governing equations and evaluate the fluctuation quantities using the polarization relations, we see that

$$\vec{u}\cdot\nabla \to u(\imath k) + w\left(\imath m + \frac{1}{2H}\right) = \imath k u + \imath m w + \frac{w}{2H}. \tag{19}$$

However, Eq. (7) gives $\imath k u + \imath m w + w/2H = 0$. Therefore, the advective terms in the fully nonlinear equations evaluate to zero, meaning that the plane wave solutions to the linear equations are also exact solutions of the fully nonlinear equations. Thus, the plane wave solutions for the linear problem are identical in form to the solutions for the nonlinear problem. As a consequence, the standard procedure first developed by Stokes to examine moderately large amplitude surface waves cannot be applied to internal waves [19].

Instead we develop a weakly nonlinear theory based upon the evolution of wavepackets. Assuming the waves are horizontally periodic but have localized structure in the vertical, we write our wavepacket in the form:

$$f = A_f(z,t)\exp[\imath(kx + mz - \omega t) + z/2H] + c.c., \tag{20}$$

where f can represent any of the basic state fields and $A_f(z,t)$ specifies the shape of the wavepacket envelope. Following the typical approach, detailed for example by Bretherton [29], we require that our wavepacket experience slow enough amplitude modulation so that the packet is quasi-monochromatic and can be treated as having a single vertical wavenumber, m, and horizontal wavenumber, k. We will consider a single wavepacket, propagating vertically at the vertical group velocity, $c_{gz} = \partial\omega/\partial m$. We restrict ourselves to a wavepacket propagating upwards, with $m/k < 0$, in order to ensure the development of weakly nonlinear effects. A small amplitude wavepacket, which obeys linear theory, will grow in amplitude and transition into the nonlinear regime as it propagates upwards, due to the decreasing background density field.

The total velocity field $\vec{u_T}(x,z,t) \equiv (U+u, w)$ is separated into the mean horizontal flow induced by the waves, $U(z,t)$, and the fluctuation velocities (u,w), which have the form (20). We substitute this into the horizontal momentum equation, Eq. (7):

$$\partial_t u_T = -\left[\partial_x(u_T u_T) + \partial_z(u_T w_T) + \frac{1}{\bar\rho}\partial_x p\right], \tag{21}$$

and note that the x-independent part of the product fg, $(A_f(A_g)^\star + (A_f)^\star A_g)\exp(z/H)$ in which the star denotes the complex conjugate, is equivalent to the horizontal average $\langle fg\rangle$. This leads to

$$\partial_t U = -\partial_z\langle uw\rangle. \tag{22}$$

The width σ of the wavepacket is assumed to be so broad that $\epsilon \equiv 1/(k\sigma) \ll 1$. Thus we define a slow spatial variable Z that translates at the vertical group velocity predicted by linear theory: $Z \equiv \epsilon(z - c_{gz}t)$. In order to balance the time evolution with the dispersion terms in Eq. (2), the corresponding slow time variable is $T \equiv \epsilon^2 t$. Putting these in (22) and extracting terms at order ϵ gives

$$c_{gz}\partial_Z U = \partial_Z\langle uw\rangle. \tag{23}$$

Finally, integration of (23) with respect to Z leads to an explicit expression for the wave-induced mean flow

$$U = \frac{1}{c_{gz}}\langle uw\rangle. \tag{24}$$

The result is identical to (5) except that here we have derived it on the basis of momentum of a wavepacket rather than wave action conservation for plane waves.

The derivation of Eq. (24) shows that the wave-induced mean flow of a wavepacket is essentially the result of horizontal momentum being transported upward at the vertical group velocity. Put another way, the vertical flux of horizontal momentum is equal to the vertical transport of the momentum associated with the wave-induced mean flow at the vertical group velocity. This is analogous to the flux of energy, which is well known to equal the transport of energy at the vertical group velocity.

Eq. (24) represents the wave-induced mean flow for a wavepacket in a Boussinesq fluid or in a non-Boussinesq liquid. In the former case, the polarization relations can be used to show that (24) is equivalent to (1), the form for the wave-induced mean flow previously derived for Boussinesq waves [3].

The wave-induced mean flow can be related to the vertical displacement amplitude of the wavepacket, A_ξ, at leading order through the use of the polarization relations for non-Boussinesq internal gravity waves, given in Table 1. Then (24) becomes

$$U = \frac{1}{2}N^2\frac{k}{\omega}|A_\xi|^2\exp(z/H). \tag{25}$$

This is given in terms of the stationary coordinate z. The time evolution of U is given by shifting to the translating coordinate Z.

We now turn our attention to the derivation of the corresponding weakly nonlinear Schrödinger equation for internal waves in a non-Boussinesq liquid. Our approach is a continuation of the procedure used to find the wave-induced mean flow. Returning to the governing equations, we take the curl of the momentum conservation equations given by (6) and, using (7), get two coupled nonlinear equations for the total streamfunction and the fluctuation density:

$$\frac{D}{Dt}\nabla^2\psi_T = -\frac{g}{\bar\rho}\frac{\partial\rho}{\partial x} - \frac{1}{\bar\rho}\frac{\mathrm{d}\bar\rho}{\mathrm{d}z}\frac{D}{Dt}\partial_z\psi_T \tag{26}$$

$$\frac{D\rho}{Dt} = -\frac{\mathrm{d}\bar\rho}{\mathrm{d}z}\frac{\partial\psi_T}{\partial x}. \tag{27}$$

In the case of uniform stratification, for which we have an exponentially decreasing background density profile, the vertical displacement of the waves, ξ, is related to the fluctuation density by

$$\xi = -H\ln\left[1 - \frac{\rho}{\bar\rho}\right] \approx H\frac{\rho}{\bar\rho}, \tag{28}$$

the approximation being valid if $|\rho/\bar\rho| \ll 1$. The vertical displacement is related to the vertical component of the fluctuation velocity by $w = \partial_t\xi$. Using the polarization relations in Table 1, we can also relate ξ to the streamfunction through $A_\xi = -(k/\omega)A_\psi$.

Our goal is to derive an approximate equation for the weakly nonlinear evolution of the wavepacket in terms of the vertical

displacement amplitude envelope $A_\xi(z,t)$. We will assume that initial weakly nonlinear effects result only from interactions between the waves and the wave-induced mean flow. Thus we write $\psi_T = \bar{\psi} + \psi$ with $U = -\partial_z\bar{\psi}$. Following the approach of [3], (26) and (20) are combined and the coefficients of the $\exp[\imath(kx + mz - \omega t) + z/2H]$ terms are extracted to give a differential equation for the streamfunction and vertical displacement amplitude envelopes, A_ξ and A_ψ:

$$\left\{[\partial_t - \imath(\omega - kU)]\left[\partial_{zz} + 2\imath m\partial_z - \kappa^2 - \frac{1}{4H^2}\right] - \imath k\left[\partial_{zz}U - \frac{1}{H}\partial_z U\right]\right\} A_\psi = -\imath k N^2 A_\xi. \tag{29}$$

Independently, (28) and (27) are combined with Eq. (20) to give a second equation for A_ξ and A_ψ:

$$[\partial_t - \imath(\omega - kU)]A_\xi = \imath k A_\psi, \tag{30}$$

in which we have once again extracted only the coefficients of the wave-like terms occurring in combination with $\exp[\imath(kx + mz - \omega t) + z/2H]$.

Eq. (30) is used to eliminate A_ψ from (29), resulting in a single differential equation for the evolution of A_ξ:

$$\left\{[\partial_t - \imath(\omega - kU)]\left[\partial_{zz} + 2\imath m\partial_z - \kappa^2 - \frac{1}{4H^2}\right] - \imath k\left[\partial_{zz}U - \frac{1}{H}\partial_z U\right]\right\} [\partial_t - \imath(\omega - kU)]A_\xi = k^2 N^2 A_\xi, \tag{31}$$

in which U is defined by (24). We transform into a frame of reference with vertical coordinate $Z \equiv \epsilon(z - c_{gz}t)$ and time coordinate $T \equiv \epsilon^2 t$.

In order to apply perturbation theory we require that the vertical width of the wavepacket be sufficiently large such that $\epsilon \equiv 1/(k\sigma) \ll 1$. For leading order dispersion to balance nonlinearity we require that the maximum vertical displacement A_{ξ_0} be large enough such that $\alpha \equiv kA_{\xi_0}$ is of order ϵ. Keeping terms up to third order in ϵ and recasting the result in terms of z and t gives the weakly nonlinear Schrödinger equation for A_ξ:

$$\partial_t A_\xi + c_{gz}\partial_z A_\xi = \imath\frac{1}{2}\omega_{mm}\partial_{zz}A_\xi + \frac{1}{6}\omega_{mmm}\partial_{zzz}A_\xi - \imath kUA_\xi + \frac{1}{2}\frac{\omega^2}{N^2 k}\left(m + \frac{\imath}{H}\right)(\partial_z U)\,A_\xi. \tag{32}$$

Here the left-hand side explicitly includes the advective derivative describing the translation of the wavepacket at the group velocity. The coefficients of the linear terms on the right-hand side are given by

$$\omega_{mm} = \frac{\omega}{\kappa^2 + \frac{1}{4H^2}}\left[\frac{3m^2}{\kappa^2 + \frac{1}{4H^2}} - 1\right],$$
$$\omega_{mmm} = \frac{-3m\omega}{\left(\kappa^2 + \frac{1}{4H^2}\right)^2}\left[\frac{5m^2}{\kappa^2 + \frac{1}{4H^2}} - 3\right], \tag{33}$$

in which $\kappa^2 \equiv k^2 + m^2$.

Comparing Eq. (32) to Eq. (2), we see it includes terms describing the translation of the wavepacket at the vertical group velocity (second term on the LHS), as well as leading order linear dispersion (first term on the RHS). The nonlinear third term on the right hand side of (32) represents the Doppler-shifting of the waves by the wave-induced mean flow. This is a type of nonlinear dispersion in which the extrinsic frequency of the waves, $\Omega = \omega - kU$, is modified by their interactions with the induced mean flow. The second term on the right hand side of (32), which is third order in ϵ, is necessary to capture the linear dispersion of waves moving close to the fastest vertical group velocity, for which $\omega_{mm} \approx 0$.

The last term on the right hand side of (32) is also a third order term accounting for nonlinear dispersion resulting from the shear associated with the wave-induced mean flow. The imaginary component of this term captures effects unique to waves in a non-Boussinesq fluid. We will show that including the third order in ϵ linear and nonlinear dispersion terms is necessary to capture the symmetry breaking observed for modulationally unstable waves.

The coefficients of the first, second and fourth terms depend upon the density scale height H, which is not the case for Boussinesq waves. With the inclusion of only the first three terms on the right-hand side of (32), in the limit $H \to \infty$, the equation becomes that for Boussinesq waves [3]. If we also neglect the third order term, we are left with a special case of the formula derived by Akylas & Tabaei [11].

3. Numerical methods

In order to determine how accurately the nonlinear Schrödinger Eq. (32) captures the evolution of a two-dimensional, vertically localized, horizontally periodic wavepacket, numerically integrated solutions of (32) will be compared with the results of fully nonlinear numerical simulations.

In both the weakly and the fully nonlinear numerical simulations, the relative space and time scales are effectively determined by setting $N = 1$ and $k = 1$. For convenience, however, we will often replace these parameters with a length scale $L = k^{-1}$ and a time scale $T = N^{-1}$. Thus, the results given here will be normalized by these parameters or, where conceptually convenient, by the horizontal wavelength $\lambda_x = 2\pi/k$. Our dimensional variables will therefore be replaced by their non-dimensional counterparts through the following substitutions:

$$\vec{x} \to L\,\vec{x}, \qquad t \to T\,t, \qquad \vec{u} \to \frac{L}{T}\,\vec{u}, \qquad \bar{\rho} \to \rho_0\,\bar{\rho}, \qquad \rho \to \rho_0\frac{L}{H}\,\rho$$

where ρ_0 is a constant characteristic density.

The fully nonlinear numerical simulation solves the following non-dimensional coupled equations for the fluctuation density, $\rho(x,z,t)$, and the 'mass-weighted' vorticity, $\eta(x,z,t) \equiv \nabla\times(\bar{\rho}\vec{u})$:

$$\frac{D\eta}{Dt} = J\frac{\partial\rho}{\partial x} + w\zeta\frac{\mathrm{d}\bar{\rho}}{\mathrm{d}z}\frac{L}{H} + wu\frac{\mathrm{d}^2\bar{\rho}}{\mathrm{d}z^2}\left(\frac{L}{H}\right)^2 + \frac{\nabla^2\zeta}{Re}, \tag{34}$$

and

$$\frac{D\rho}{Dt} = -w\frac{\mathrm{d}\bar{\rho}}{\mathrm{d}z} + \frac{\nabla^2\rho}{RePr} \tag{35}$$

where $\zeta = \nabla\times\vec{u} = -\nabla^2\psi$ is the vorticity field of the waves. Eq. (34) is derived by taking the curl of Eq. (6), and casting the result in terms of η for numerical convenience. It is equivalent to Eq. (26), and its dimensional form can be converted to that equation by relating η to the streamfunction:

$$\eta = -\bar{\rho}\nabla^2\psi - \frac{\mathrm{d}\bar{\rho}}{\mathrm{d}z}\frac{\partial\psi}{\partial z}. \tag{36}$$

In this circumstance, the bulk Richardson number, describing the ratio of the buoyancy to the inertia forces in the fluid [1], is $J \equiv \frac{g}{H}T^2 = \frac{g}{H}N^{-2} = 1$.

Eqs. (34) and (35) include diffusion terms that act to damp small-scale noise in order to maintain numerical stability during wave breaking. The Prandtl number is set to be $Pr = 1$. The

Table 2
Relevant parameters and coefficients of (32) for the simulations presented herein.

m/k	Θ (°)	ω/N	$c_{gz}\frac{k}{N}$	$\omega_{mm}\frac{k^2}{N}$	$\omega_{mmm}\frac{k^3}{N}$	$U_0\frac{k}{N}$	$U_{\text{Max}}\frac{k}{N}$
−0.4	−21.8	0.93	0.32	−0.470	−1.91	0.0026	0.19
−0.7	−35.0	0.82	0.38	−0.008	−1.05	0.0029	0.22
−1.4	−54.5	0.58	0.27	0.193	0.09	0.0041	0.06

Reynolds number is set to be $Re \equiv \frac{\nu k^2}{N} = 10\,000$. Both Re and $RePr$ are chosen to be sufficiently large such that diffusion negligibly affects the wave evolution. No significant changes in the wave evolution were found by decreasing the Reynolds number to 5000.

The simulation is spectral in the horizontal and uses a second order finite-difference scheme to perform vertical derivatives. It progresses in time using the 'leap-frog' method, with an Euler backstep taken every 20 timesteps. In the vertical the domain resolution is 1024 grid points. In the horizontal the wavenumbers are resolved down to $8k$. The wavepacket is initialized at the origin of the vertical domain, which extends from $z = -150k^{-1}$ to $150k^{-1}$. The upper and lower boundary conditions are free slip. However, the vertical domain is chosen to be large enough that the waves are of negligibly small amplitude at the boundaries over the duration of each simulation. The horizontal extent of the domain is $\lambda_x = 2\pi/k$. The simulations were allowed to run from $t = 0$, with a timestep of $0.025N^{-1}$, until wave breaking occurred, generally about 40–60 buoyancy periods. The period of interest for the development of weakly nonlinear effects generally occurred between $t = 100N^{-1}$ and $t = 250N^{-1}$. Doubling the resolution was found to have no significant qualitative or quantitative effect on the wave dynamics.

The initial parameters for the simulations considered here are provided in Table 2. We simulate wavepackets with a range of vertical wavenumbers, encompassing hydrostatic waves, for which $\partial p/\partial z \approx -\rho g$, as well as non-hydrostatic waves. Our wavepackets take the form of (20), with the Gaussian wavepacket envelope given by $A_f(z, 0) = \frac{1}{2}A_{f_0}\exp\left(-z^2/2\sigma^2\right)$. In all cases the waves start with relatively small amplitude and are allowed to propagate vertically upwards. An initial exponential increase in amplitude as predicted by linear theory followed by the development of weakly nonlinear effects is anticipated. The initial vertical displacement amplitude of the wavepackets is $\alpha \equiv A_{\xi_0}k = 0.07$. The extension of our results to waves of other sufficiently small initial amplitudes is given in Appendix A.

The initial wave-induced mean flow is calculated from (24). Calculation of the vertical displacement field is done using (28), with the condition $|\rho/\bar{\rho}| \ll 1$ being verified numerically at each timestep for each value of the fluctuation density. The vertical extent of the wavepacket is $\sigma = 10k^{-1}$ for the simulations presented herein, corresponding to $\epsilon = 0.1$. Doubling the vertical extent did not have a significant qualitative effect on the dominant characteristics of the weakly nonlinear evolution of the wavepacket although, as expected from the Schrödinger equation, it did increase the time scale for the development of linear dispersion and nonlinear effects.

4. Results

The modulational stability regimes of the wavepacket correspond to what is observed for large amplitude Boussinesq wavepackets [3]. A wave is modulationally unstable [19] if $\omega_{mm}\omega_2 < 0$, where ω_{mm} denotes the second derivative of frequency with respect to the vertical wavenumber, and ω_2 is the coefficient of the $-\imath|A|^2A$ term in (32):

$$\omega_2 = \frac{1}{2}N^2\frac{k^2}{\omega_0}. \tag{37}$$

Because $\omega_2 > 0$ for internal gravity waves, modulational stability is determined by the sign of ω_{mm}. This term is negative if $|m| < 2^{-1/2}(k^2 + \frac{1}{4H^2})^{1/2}$, which results in modulational instability, and is positive otherwise. The critical point between modulational stability and instability occurs for waves with fixed k moving at the fastest initial vertical group velocity. For the range of density scale heights considered in this work, which fall between $H = 0.5\lambda_x$ and $H = 10.0\lambda_x$, this corresponds to $|m/k| \simeq 2^{-1/2} \approx 0.71$.

First the results from the fully nonlinear numerical simulations will be considered. Fig. 1 shows the evolution of the vertical displacement field of the waves at early, late, and very late times for a non-hydrostatic wavepacket with vertical wavenumber $m = -0.4k$. For each time, the left-hand panel contains a contour plot of the normalized vertical displacement, ξk, and the right-hand panel shows the corresponding shape of the normalized vertical displacement amplitude envelope, $|A_\xi|k$. The packet is initially of small amplitude with $\alpha \equiv kA_{\xi_0} = 0.07$. The density scale height is $H = 3.2\lambda_x$.

Fig. 1(a) shows the wavepacket at $t = 100N^{-1}$, before the onset of weakly nonlinear effects. The amplitude has increased as predicted by linear theory, growing exponentially with height to $\|A_\xi\| = 0.15k^{-1}$. In Fig. 1(b), we see the wavepacket during the onset of weakly nonlinear effects at $t = 175N^{-1}$. The wavepacket envelope has narrowed, become more peaked, and is no longer symmetrical. This is consistent with the wavepacket being modulationally unstable. The amplitude has increased to $\|A_\xi\| = 0.35k^{-1}$, substantially larger than the value predicted by linear theory, $0.28k^{-1}$.

Fig. 1(c) shows the evolution of the wavepacket at very late times, $t = 300N^{-1}$, when the wave is beginning to overturn. Since the wavepacket is modulationally unstable, the amplitude envelope has narrowed sharply and has experienced a rapid increase in amplitude. Its maximum is now $\|A_\xi\| = 0.85k^{-1}$, about 10% larger than the value of $\|A_\xi\| = 0.77k^{-1}$ predicted by linear theory. Due to these weakly nonlinear effects, the wavepacket begins to overturn at a lower height than predicted by linear theory, indicated in the figure by the thick black line at $z = 22.7\lambda_x$. Wave breaking actually occurs about 50% lower, at $z = 11.4\lambda_x$.

Fig. 2 is identical to Fig. 1, except that it shows the vertical displacement field of a wavepacket on the cusp between modulational stability and instability, with vertical wavenumber $m = -0.7k$. In Fig. 2(a), the amplitude of the envelope at $t = 100N^{-1}$ has increased as predicted by linear theory. In Fig. 2(b), weakly nonlinear effects have developed at $t = 175N^{-1}$: the amplitude envelope has narrowed and lost its vertical symmetry. However, the maximum amplitude shows an increase consistent with linear theory.

Fig. 2(c) shows the wavepacket development at $t = 250N^{-1}$, which is during wave breaking. Since this wavepacket propagates with the largest initial vertical group velocity, it reaches its breaking level most rapidly. The amplitude envelope has divided into several distinct peaks, with a maximum of $\|A_\xi\| = 0.78k^{-1}$. This is close to the value given by linear theory, $\|A_\xi\| = 0.75k^{-1}$. The wavepacket first breaks at $z = 12.8\lambda_x$, much lower than the predicted height of $z = 19.2\lambda_x$ indicated by the black line. This is a decrease in breaking height of slightly more than 30%.

Fig. 3 contains a more hydrostatic wavepacket with vertical wavenumber $m = -1.4k$, which is expected to be modulationally stable. The wavepacket is shown at early times in Fig. 3(a), with $t = 100N^{-1}$. Due to modulational stability, the amplitude of the wavepacket envelope is slightly lower than that predicted by linear theory, with a value of $\|A_\xi\| = 0.13k^{-1}$ as compared to $\|A_\xi\| = 0.14k^{-1}$. Fig. 3(b) shows the modulationally stable wavepacket at a later time during its development, $t = 175N^{-1}$, at which point it has broadened significantly, and become slightly asymmetrical.

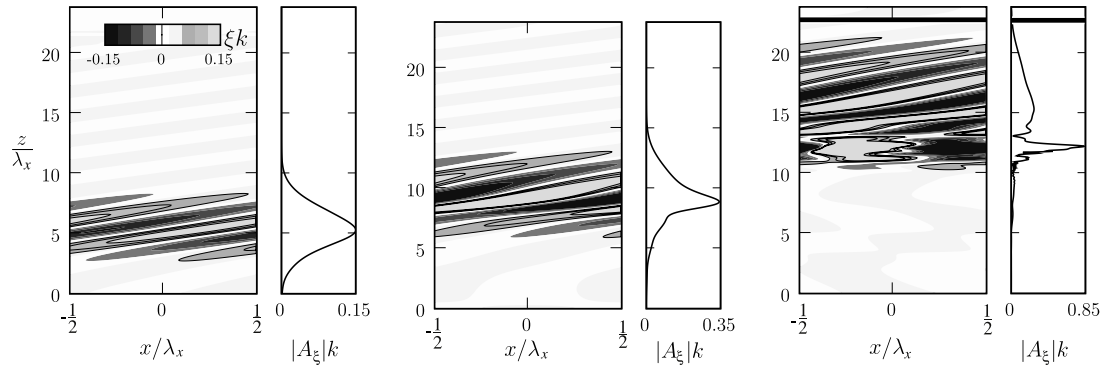

(a) $t = 100/N^{-1}$. (b) $t = 175/N^{-1}$. (c) $t = 300/N^{-1}$.

Fig. 1. Left-hand panels show contour plots of the normalized vertical displacement field, $\xi(x, z, t)\,k$, and right-hand panels show the corresponding normalized wavepacket amplitude envelope, $|A_\xi|k$, from fully nonlinear simulations with $H = 3.2\lambda_x$, $\alpha \equiv kA_{\xi_0} = 0.07$ and $m = -0.4k$. The wavepacket evolution is shown for (a) $t = 100N^{-1}$, (b) $t = 175N^{-1}$, and (c) $t = 300N^{-1}$. The horizontal black line indicates the breaking level predicted by linear theory.

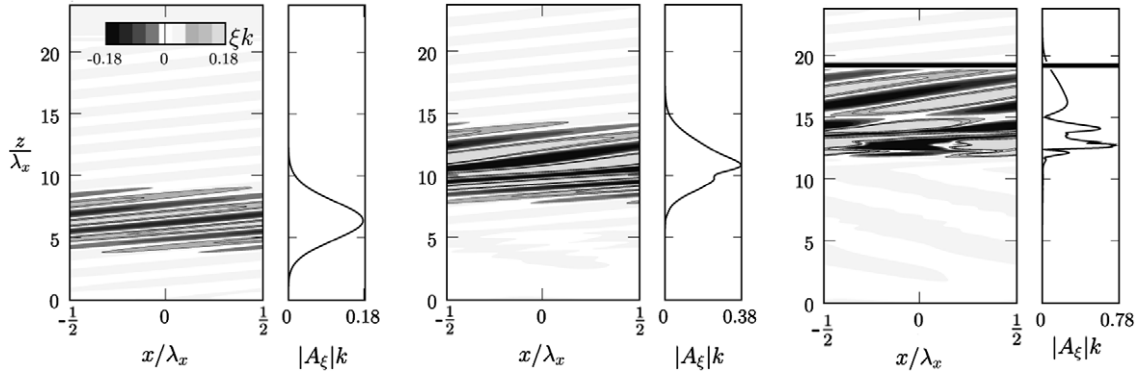

(a) $t = 100/N^{-1}$. (b) $t = 175/N^{-1}$. (c) $t = 250/N^{-1}$.

Fig. 2. As in Fig. 1, but for $m = -0.7k$. Times shown are (a) $t = 100N^{-1}$, (b) $t = 175N^{-1}$, and (c) $t = 250N^{-1}$. The black line indicates the breaking level predicted by linear theory.

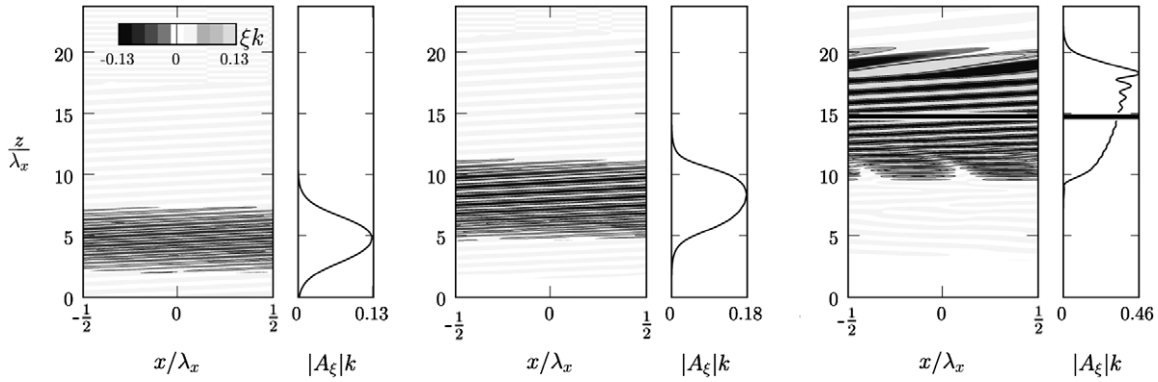

(a) $t = 100/N^{-1}$. (b) $t = 175/N^{-1}$. (c) $t = 325/N^{-1}$.

Fig. 3. As in Figs. 1 and 2, but for $m = -1.4k$. Times shown are (a) $t = 100N^{-1}$, (b) $t = 175N^{-1}$, and (c) $t = 325N^{-1}$. The horizontal black line indicates the breaking level predicted by linear theory.

The amplitude has increased to $\|A_\xi\| = 0.18k^{-1}$, which is much smaller than the value of $0.23\,k^{-1}$ predicted by linear theory.

Fig. 3(c) shows the wavepacket at time $t = 325N^{-1}$. The wavepacket is not overturning. The maximum amplitude is $\|A_\xi\| = 0.46k^{-1}$, much smaller than the predicted value of $0.63k^{-1}$. In a fully nonlinear simulation with a larger vertical domain, wave breaking was seen to occur at a height of $z = 19.5\lambda_x$. This is almost 25% higher than the breaking level given by linear theory, $z = 14.8\lambda_x$, indicated by the black line. This increase in the height of the initial overturning event is a consequence of the modulational stability of the wavepacket. The amplitude envelope has lost its vertical symmetry with a large peak at the leading edge followed by several smaller peaks. Symmetry breaking is thus apparent at late times for all three vertical wavenumbers.

We now consider the wave-induced mean flow field from the fully nonlinear numerical simulations. Fig. 4 shows time series of the normalized wave-induced mean flow for a wavepacket initialized at small amplitude $\alpha \equiv kA_{\xi_0} = 0.07$ and allowed to propagate upwards in a non-Boussinesq background with $H = 3.2\lambda_x$. The wave-induced mean flow is calculated from (24) at successive times. The three plots correspond to vertical wavenumbers of $m = -0.4k$, $-0.7k$ and $-1.4k$. For all

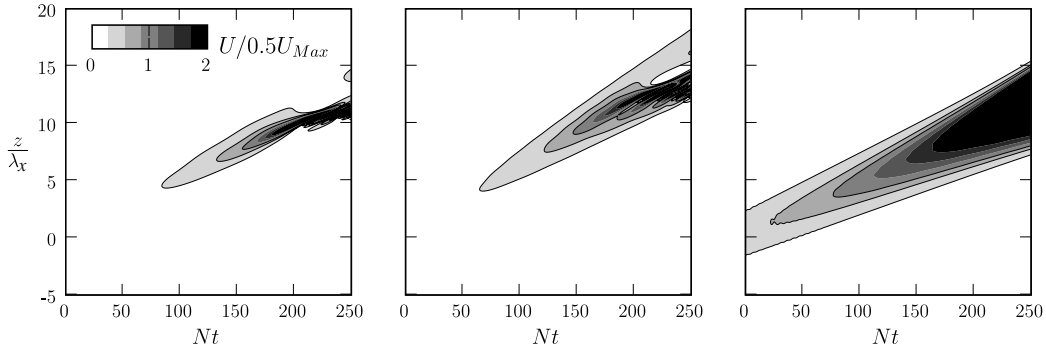

(a) $m = -0.4k$. (b) $m = -0.7k$. (c) $m = -1.4k$.

Fig. 4. Time series of the normalized wave-induced mean flow field, $U(z,t)/0.5U_{\text{Max}}$, from fully nonlinear simulations with $\alpha \equiv kA_{\xi_0} = 0.07$ and (a) $m = -0.4k$, (b) $m = -0.7k$, (c) $m = -1.4k$. U_{Max} is the maximum value of the wave-induced mean flow between $t = 0$ and $250N^{-1}$.

three, the exponential increase in wave amplitude with height is immediately visible and dominates the wave evolution.

In order to visualize more clearly the details of the wave evolution, Fig. 5 shows time series of the normalized wave-induced mean flow multiplied by the background density profile, $\bar{\rho}(Z)U(Z,t)/\rho_0 U_0$. This is shown translated into a frame moving at the initial vertical group velocity of the wavepacket predicted by linear theory. Here U_0 is the maximum value of the wave-induced mean flow field at time $t = 0$. Multiplication by $\bar{\rho}$ essentially removes the initial exponential growth associated with a non-Boussinesq wavepacket and serves to emphasize that the momentum associated with the wave-induced mean flow is conserved.

Fig. 5 therefore captures the details of the nonlinear evolution of the wavepacket with time, showing changes in the width and relative amplitude of the wave as weakly nonlinear effects develop. There are some small superimposed oscillations visible at early times that occur due to the approximations used to initialize the wavepacket, as discussed in Section 2. They have no effect on the evolution of the wavepacket at later times.

For each of the three wavenumbers presented, the evolution of the wavepacket at late times is qualitatively different. During the first part of each wavepacket's upward propagation, it moves at a near constant speed equal to the initial vertical group velocity and remains of small enough amplitude that it can be treated as being in the linear regime, as discussed for Fig. 1(a), 2a and 3a. However, between times $t = 100N^{-1}$ and $150N^{-1}$ the influence of weakly nonlinear effects becomes apparent. For a non-hydrostatic wavepacket with a vertical wavenumber of $m = -0.4k$, OR (Fig. 5(a)), the envelope of the wave-induced mean flow field associated with the wavepacket narrows while the relative amplitude increases significantly as a result of modulational instability. At late times, the wave is seen to propagate vertically at a velocity of roughly $0.26Nk^{-1}$, lower than the initial vertical group velocity of $c_{gz} = 0.32Nk^{-1}$, and symmetry breaking is observed.

For a vertical wavenumber of $m = -1.4k$, OR (Fig. 5(c)), the wave-induced mean flow envelope broadens while the peak amplitude decreases due to dispersion. These weakly nonlinear effects were also seen to occur in Fig. 3(b) and (c), as a result of the modulational stability of the wavepacket. At late times, there is some slight symmetry breaking, although very little change in the group velocity is observed. For a vertical wavenumber of $m = -0.7k$, Fig. 5(b) shows the near-marginal case between modulational stability and instability. The wavepacket broadens slightly before narrowing and increasing in amplitude. At late times, the wavepacket translates vertically more slowly than its initial vertical group velocity. Thus this wavepacket demonstrates characteristics of both modulationally stable and unstable wavepackets.

The results from integrating the solution of the weakly nonlinear Schrödinger equation are shown in Fig. 6. This equation clearly captures many of the dominant qualitative and quantitative features of the weakly nonlinear wavepacket evolution, for all three vertical wavenumbers. As with the fully nonlinear simulations, the non-hydrostatic wave (Fig. 6(a)) narrows and increases in amplitude due to modulational instability. The more hydrostatic wave (Fig. 6(c)) broadens and decreases in amplitude indicating that it is modulationally stable. The symmetry breaking and decrease in vertical acceleration is also captured, due to the inclusion of third order in ϵ linear and nonlinear terms in the weakly nonlinear equation. As the wavepacket narrows, the third order z-derivative terms become comparable in magnitude to the second order z-derivative term. Furthermore, due to the relatively small value of the density scale height, $H = 3.2\lambda_x$, the fourth term in the weakly nonlinear equation, which captures effects unique to waves in a non-Boussinesq fluid, contributes non-negligibly to the symmetry breaking and nonlinear evolution of the wavepacket.

Fig. 6 also demonstrates the importance of the wave-induced mean flow to wavepacket evolution. This figure clearly indicates that interactions between the waves and the wave-induced mean flow are the principal mechanism for the development of the weakly nonlinear effects that determine the dynamics of the wavepacket at late times, including its modulational stability or instability. In fact, the weakly nonlinear equation is a reasonable approximation to the fully nonlinear simulation even at very late times, capturing many of the qualitative, if not the quantitative, dynamics of the waves.

At very late times, discrepancies arise due to the appearance of parametric subharmonic instability in the fully nonlinear results. Such dynamics are not captured by the weakly nonlinear equation. It is also clear that at very late times the wave-induced mean flow field is over predicted by the weakly nonlinear equation. These quantitative differences are visible for all three wavenumbers examined herein. They are particularly clear in Fig. 6(b), which shows up to a 30% increase in amplitude over that of Fig. 5(b).

While the evolution of non-Boussinesq wavepackets is qualitatively similar to that of large amplitude Boussinesq waves, it differs in some important and related respects. As a wavepacket propagates upwards through a non-Boussinesq fluid it grows in amplitude due to the decreasing background density, as demonstrated in Fig. 4. This is not the case for waves initialized at small amplitude in a Boussinesq fluid, which decrease slightly in amplitude due to linear dispersion but remain otherwise unchanged. Thus, in order to observe the development of weakly nonlinear effects in a Boussinesq fluid, a wavepacket must be initially of large amplitude. On the contrary, a wavepacket in a non-Boussinesq fluid may be initialized at small amplitude and allowed to grow in amplitude to such a point that weakly nonlinear dynamics are observed.

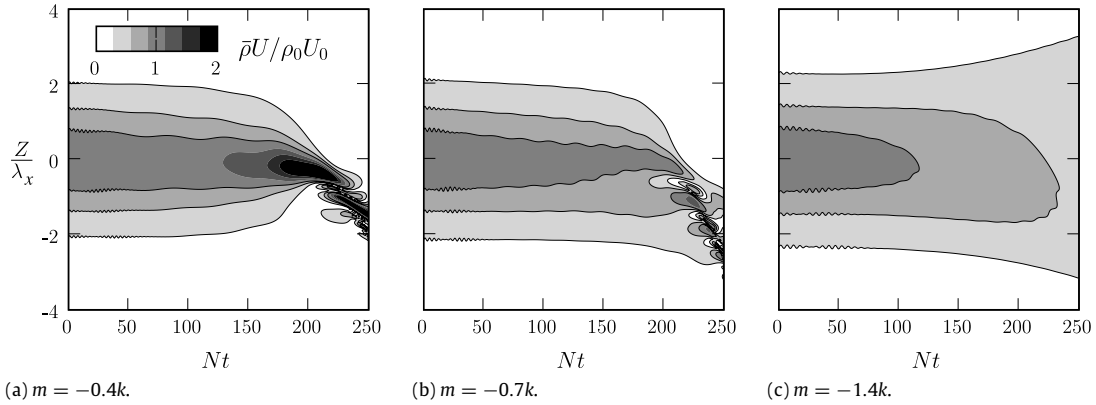

(a) $m = -0.4k$. (b) $m = -0.7k$. (c) $m = -1.4k$.

Fig. 5. Time series from fully nonlinear numerical simulations of the normalized wave-induced mean flow field multiplied by the background density profile, $\bar{\rho}(Z)U(Z,t)/\rho_0 U_0$, with $\alpha \equiv kA_{\xi_0} = 0.07$ and (a) $m = -0.4k$, (b) $m = -0.7k$, (c) $m = -1.4k$. Here $Z = z - c_{gz}t$ is the coordinate translating at the vertical group velocity, and Nt is the normalized time coordinate.

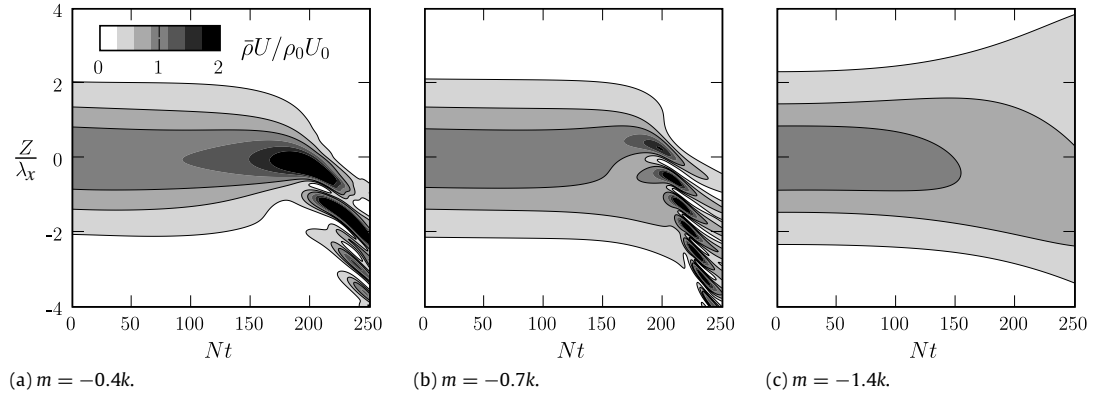

(a) $m = -0.4k$. (b) $m = -0.7k$. (c) $m = -1.4k$.

Fig. 6. As in Fig. 5, but for $\bar{\rho}U/\rho_0 U_0$ from solutions of the weakly nonlinear Schrödinger equation. Wavenumbers shown are (a) $m = -0.4k$, (b) $m = -0.7k$, and (c) $m = -1.4k$.

The Schrödinger equation for non-Boussinesq waves is thus able to capture both the weakly nonlinear evolution of the wavepacket and the transition of the waves from the linear to the nonlinear regimes.

5. Breaking levels

In order to gain further insight into the influence of nonlinear effects on wave evolution at late times, fully nonlinear numerical simulations were performed in which the wavepackets were allowed to propagate vertically towards the breaking level predicted by linear theory. The condition for wave overturning is given by

$$\frac{\partial \rho}{\partial z} + \frac{\mathrm{d}\bar{\rho}}{\mathrm{d}z} > 0. \tag{38}$$

The left-hand side of this expression was calculated at each vertical level in the domain at each timestep. The lowest vertical level at which overturning occurred was denoted as the breaking height z_B. This height can be compared with the breaking height z_{B0} predicted by linear theory.

For an internal gravity plane wave in an exponentially decreasing non-Boussinesq background stratification this condition is given in terms of the vertical displacement amplitude of the wave by:

$$-A_{\xi_0} \exp[z/2H] \max[m\ \sin(kx + mz - \omega t) + \frac{1}{2H}\cos(kx + mz - \omega t)] > 1. \tag{39}$$

The predicted breaking height from linear theory, z_{B0}, can be calculated from this expression for a given density scale height, H, and vertical wavenumber, m. It is acceptable to use the breaking condition for a plane wave, rather than for a wavepacket, since the width of the wavepackets considered was large enough that any correction to this formula would be negligible. Test cases (not shown), in which the width of the wavepackets was doubled, demonstrated slightly increased breaking heights to those presented herein. However, the overall trends in relation to linear theory were not significantly affected.

Fig. 7 compares the predicted breaking heights z_{B0} with the breaking heights z_B determined from the fully nonlinear numerical simulations for a range of λ_x/H. For waves of wavenumber $m = -0.4k$, breaking occurs consistently below the levels predicted by linear theory. This is as expected because modulational instability causes the amplitude of the waves to grow at a rate faster than expected from linear theory. Conversely, modulationally stable waves of wavenumber $m = -1.4k$ break well above the predicted levels. Waves with vertical wavenumber $m = -0.7k$ are on the cusp between modulational stability and instability. They demonstrate breaking both above and below the heights predicted by linear theory, depending upon the value of λ_x/H.

If we consider λ_x to be fixed, and allow H to vary, we see that for the range of density scale heights considered, agreement with linear theory improves for waves in increasingly non-Boussinesq fluids. There is some indication in Fig. 7(b) that this trend may reverse as H becomes increasingly small. We were unable to confirm this using the numerical model, however, as the wavepackets became unstable and began to overturn almost immediately upon initialization. It is also clear from Fig. 7 that

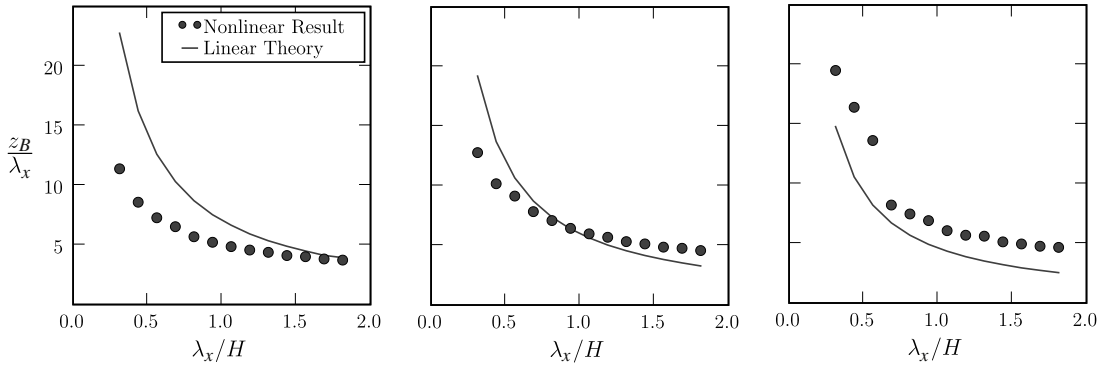

(a) $m = -0.4k$. (b) $m = -0.7k$. (c) $m = -1.4k$.

Fig. 7. Results from fully nonlinear numerical simulations for the normalized breaking height z_B/λ_x of a wavepacket with $\alpha \equiv kA_{\tilde{w}_0} = 0.07$, plotted against the horizontal wavelength normalized by the density scale height λ_x/H. The vertical wavenumbers shown are $m = -0.4k$, $m = -0.7k$, and $m = -1.4k$. The solid lines are theoretical predictions from linear theory.

waves in more Boussinesq fluids are able to propagate further before breaking, which is consistent with our expectations of decreased amplitude growth for larger density scale heights.

6. Conclusions

As a step to understanding the evolution of anelastically growing, upward propagating internal waves in the atmosphere, we have performed a theoretical and numerical study of internal wavepackets in a non-Boussinesq liquid. This system of equations has been chosen as a starting point in part because it constitutes a straightforward extension of the Boussinesq equations, with density representing the thermodynamics, and because it provides a testing ground for eventual comparison with laboratory experiments using high-density solutions of salts such as sodium iodide [30].

It has been shown that the dominant characteristics of the early evolution of a horizontally periodic, vertically localized wavepacket are well captured in both the linear and nonlinear regimes by a weakly nonlinear Schrödinger equation describing only the interactions of the waves with the wave-induced mean flow. In fact, the Schrödinger equation is a reasonably good approximation even at late times. If $Hk \gg 1$, waves of frequency $\omega \gtrsim 2^{-1/2}N$ are modulationally unstable, experiencing growth and narrowing of the amplitude envelope and a decrease in vertical group velocity. Modulationally stable waves with $\omega < 2^{-1/2}N$ experience rapid broadening and decreasing relative amplitude. In order to capture the symmetry breaking and decreased propagation speed associated with modulationally unstable waves, it was necessary to include third order terms in the weakly nonlinear Schrödinger equation. This symmetry breaking is also seen for waves of frequency $\omega \approx 2^{-1/2}N$, which propagate at the fastest vertical group velocity and represent the critical point between modulational stability and instability. At very late times, it was seen that the weakly nonlinear equation, while still capturing many of the qualitative features of the wavepacket evolution, was unable to predict correctly some of the quantitative features of the waves. In particular, the maximum amplitude of the wave-induced mean flow field was too large when compared to the results of the fully nonlinear numerical simulations. Overall, it was found that the weakly nonlinear dynamics of internal waves in a non-Boussinesq fluid are entirely determined by the interaction of the waves with the wave-induced mean flow at early times, with parametric subharmonic instability occurring only at very late times.

These results have important implications for internal gravity wave breaking in non-Boussinesq fluids: non-hydrostatic waves ($\omega \gtrsim 2^{-1/2}N$) consistently break at lower levels than predicted by linear theory; hydrostatic waves break at heights greater than those predicted by linear theory. Hence, for a given scale height H, linear theory does not correctly predict the breaking height for most circumstances. As an illustration, consider hydrostatic internal waves having horizontal wavelength on the order of 10 km. Fig. 7 indicates that such waves will break on the order of $1\frac{1}{2}$ times higher than predicted by linear theory. This result indicates that general circulation models of the atmosphere that use linear theory to parameterize hydrostatic wave breaking likely deposit momentum too low down in the atmosphere.

Ongoing research will extend this analysis to an anelastic gas and will include the effects of non-uniform background flows and stratifications. This will provide a more realistic representation of internal gravity wave propagation, weakly nonlinear wave evolution and fully nonlinear wave breaking in anelastic fluids such as the atmosphere.

Acknowledgements

The research from which this work resulted was supported by the Natural Sciences and Engineering Research Council of Canada (NSERC), and the Canadian Foundation for Climate and the Atmospheric Sciences (CFCAS).

Appendix A

The results presented in Fig. 7 are for one particular wavepacket amplitude, $\alpha = 0.07$. It is possible to extend these results to any wavepacket of small initial amplitude, which in practice means $\alpha \lesssim 0.2$. Assuming that at early times the wavepacket has relatively small amplitude and evolves linearly, growing only as a result of the exponential decrease in background density, a new breaking height $z_{B^\star}$ can be predicted from the known data for z_B. For a wavepacket of amplitude $\alpha^\star$, the new breaking height is given approximately by

$$z_{B^\star} = z_B - 2H \ln\left(\frac{\alpha^\star}{\alpha}\right), \tag{A.1}$$

in which z_B is the breaking height determined from a simulation of a wavepacket with initial amplitude α. For example, for a wavepacket with $\alpha^\star = 0.10$, $m = -1.4k$ and $\lambda_x/H = 0.3$, Eq. (A.1) predicts that $z_{B^\star} = 17.2\lambda_x$. A fully nonlinear numerical simulation gives a value of $z_B = 16.9\lambda_x$ while linear theory predicts $z_{B0} = 12.5\lambda_x$. Thus, even approximating the breaking height from available nonlinear data represents a significant improvement over the use of linear theory.

References

[1] P.K. Kundu, Fluid Mechanics, Academic Press, San Diego, 1990.
[2] A. Eliassen, E. Palm, On the Transfer of Energy in Stationary Mountain Waves, Geofys. Publ. 22 (1961) 1–23.
[3] B.R. Sutherland, Weakly nonlinear internal wavepackets, J. Fluid Mech. 569 (2006) 249–258.
[4] T.J. Dunkerton, Wave transience in a compressible atmosphere. part I: transient internal wave, mean-flow interaction, J. Atmos. Sci. 38 (1981) 281–297.
[5] R.H.J. Grimshaw, Nonlinear internal gravity waves and their interaction with the mean wind, J. Atmos. Sci. 32 (1975) 1779–1793.
[6] W.L. Jones, D.D. Houghton, The self-destructing internal gravity wave, J. Atmos. Sci. 29 (1972) 844–849.
[7] J.F. Scinocca, T.G. Shepherd, Nonlinear wave-activity conservation laws and Hamiltonian structure for the two-dimensional anelastic equations, J. Atmos. Sci. 49 (1992) 5–27.
[8] M.E. McIntyre, On the wave momentum myth, J. Fluid Mech. 106 (1981) 331–347.
[9] B.R. Sutherland, Internal gravity wave radiation into weakly stratified fluid, Phys. Fluids 8 (1996) 430–441.
[10] B.R. Sutherland, Internal wave instability: wave–wave vs wave-induced mean flow interactions, Phys. Fluids. 18 (074107) (2006) doi:10.1063/1.2219102.
[11] T.R. Akylas, A. Tabaei, Resonant self-acceleration and instability of nonlinear internal gravity wavetrains, in: A. Litvak (Ed.), Frontiers of Nonlinear Physics, Institute of Applied Physics, 2005, pp. 129–135.
[12] D.C. Fritts, T.J. Dunkerton, A quasi-linear study of gravity-wave saturation and self-acceleration, J. Atmos. Sci. 41 (1984) 3272–3289.
[13] B.R. Sutherland, Propagation and reflection of large amplitude internal gravity waves, Phys. Fluids 11 (1999) 1081–1090.
[14] B.R. Sutherland, Finite-amplitude internal wavepacket dispersion and breaking, J. Fluid Mech. 429 (2001) 343–380.
[15] F.P. Bretherton, On the mean motion induced by internal gravity waves, J. Fluid Mech. 36 (1969) 785–803.
[16] A.E. Gill, Atmosphere-Ocean Dynamics, Academic Press, San Diego, 1982.
[17] D.J. Acheson, On over-reflexion, J. Fluid Mech. 77 (1976) 433–472.
[18] D.G. Andrews, M.E. McIntyre, An exact theory of nonlinear waves on a Lagrangian-mean flow, J. Fluid Mech. 89 (1978) 609–646.
[19] G.B. Whitham, Linear and Nonlinear Waves, John Wiley and Sons, Inc., New York, 1974.
[20] O.M. Phillips, Wave interactions—the evolution of an idea, J. Fluid Mech. 106 (1981) 215–227.
[21] E. Fermi, J. Pasta, S. Ulam, Studies of nonlinear problems I, los alamos report LA 1940, 1955, in: A.C. Newell (Ed.), (reproduced) Nonlinear Wave Motion, Amer. Math. Soc., Providence, RI, 1974.
[22] B.M. Lake, H.C. Yuen, H. Rundgaldier, W.E. Ferguson, Nonlinear deep-water waves: theory and experiment, part 2, evolution of a continuous wave train, J. Fluid Mech. 83 (1977) 49–74.
[23] T.B. Benjamin, J.E. Feir, The disintegration of wavetrains on deep water, J. Fluid Mech. 27 (1967) 417–430.
[24] Dysthe, Note on a modification of the nonlinear Schrödinger equation for application to deep water waves, Proc. Roy. Soc. A 369 (1979) 105–114.
[25] J. Klostermeyer, Two- and three-dimensional parametric instabilities in finite amplitude internal gravity waves, Geophys. Astrophys. Fluid Dyn. 64 (1991) 1–25.
[26] P.N. Lombard, J.J. Riley, On the breakdown into turbulence of propagating internal waves, Dyn. Atmos. Oceans 23 (1996) 345–355.
[27] P. Bouruet-Aubertot, J. Sommeria, C. Staquet, Breaking of standing internal gravity waves through two-dimensional instabilities, J. Fluid Mech. 285 (1995) 265–301.
[28] G.K. Vallis, Atmospheric and Oceanic Fluid Dynamics, Cambridge University Press, Cambridge, 2006.
[29] F.P. Bretherton, Gravity waves in shear, Quart. J. Roy. Meteorol. Soc. 92 (1966) 466–480.
[30] H.A. Clark, B.R. Sutherland, Schlieren measurements of internal waves in non-Boussinesq fluids, Expt. in Fluids 47 (2009) 183–190.